

PACS numbers: 42.68.Mj; 42.68.Wt; 42.25.Dd
DOI: 10.1070/QE2015v045n02ABEH015614

Optical-beam wavefront control based on the atmospheric backscatter signal

V.A. Banakh, V.V. Zhmilevskii, A.B. Ignatiev, V.V. Morozov, I.A. Razenkov, A.P. Rostov, R.Sh. Tsvyk

Abstract. **The feasibility of compensating for aberrations of the optical-beam initial wavefront by aperture sounding, based on the atmospheric backscatter signal from an additional laser source with a different wavelength, is experimentally studied. It is shown that the adaptive system based on this principle makes it possible to compensate for distortions of the initial beam wavefront on a surface path in atmosphere. Specifically, the beam divergence decreases, while the level of the detected mean backscatter power from the additional laser source increases.**

Keywords: *wavefront, compensation, atmospheric backscatter.*

1. Introduction

When generating high-power laser beams, elements of the optical channel may undergo thermal strains, as a result of which the beam wavefront at the output aperture of the transmitting telescope acquires an uncontrolled random deviation from specified distribution. The beam becomes partially spatially coherent, and its divergence may significantly exceed the diffraction divergence. Correspondingly, the power density in the paraxial region of the beam cross section decreases. For laser beams propagating in atmosphere, the distorting effect of turbulent fluctuations of the refractive index decreases with increasing radiation wavelength, and, in the case of IR laser beams, the increase in their transverse size due to the incomplete spatial coherence of the initial field may be comparable with the turbulent beam broadening or even exceed it. The influence of thermal aberrations on the beam quality is even more pronounced on inclined and high-altitude paths, because optical turbulence intensity decreases with increasing height. On these paths, the wavefront distortions caused by thermal aberrations begin to play a key role in the decrease in the radiation power arriving at the detector. Thus, one has to suppress these initial 'intrinsic' aberrations (i.e., improve the initial wavefront of a partially coherent beam at the output aperture).

The use of a wavefront sensor for generating a signal to control an adaptive mirror in order to compensate for distortions of the initial wavefront leads to significant complication of the beam-formation system, incorporation of diffractive couplers into the optical scheme, necessity of reconstructing the phase based on amplitude data, etc.; all these problems cannot always be successfully solved. As an alternative version, it was proposed to use atmosphere as a wavefront sensor in [1]. Indeed, when a laser beam propagates in atmosphere, it undergoes aerosol and molecular scattering. The scattering phase function depends on the beam wavelength; however, the beam is always partially backscattered. The scattered power depends on the propagating beam power. The beam divergence caused by thermal aberrations reduces the power density. Thus, when a narrow-field-of-view detector is used to record backscattered radiation, the detected power is sensitive to variations in the beam divergence and can be used to control the adaptive mirror.

A further development of this concept was related to the idea of controlling the mirror by scattered radiation of some auxiliary (probe) beam rather than the beam under consideration (the main beam). The point is that the backscatter power is low, and the backscatter signal cannot always be detected. However, introduction of a probe beam (the wavefront of which is expected to acquire the same distortions as the main beam) into the optical channel and focusing it at some short distance in atmosphere provide a backscatter signal from the beam waist sufficiently large to be recorded by existing detectors.

The problem of compensating for distortions of the initial wavefront of a partially coherent light beam using an atmospheric backscatter signal for adaptive-mirror control was considered theoretically in [2–4]. Based on computer simulation, the possibility of correcting the initial wavefront was analysed in detail, and requirements to the transceiver parameters, providing compensation for wavefront distortions by this method were determined in these studies. In [5], we reported the results of atmospheric experiments aimed at compensating for beam-phase initial distortions by aperture sounding [using a stochastic parallel gradient descent (SPGD) algorithm [6, 7] for mirror control] over the peak power of screen-scattered detected radiation.

In this paper, we report the results of natural experiments aimed at compensating for aberrations of the initial wavefront of a partially coherent (main) laser beam by aperture sounding [8, 9], based on the atmospheric backscatter signal of another (probe) beam with a different wavelength but transmitted through the same optical channel and acquired the same wavefront distortions as the main beam.

2. Optical scheme of the experimental setup

Experiments were performed on a specially designed setup implementing the aperture sounding method. The main and

V.A. Banakh, I.A. Razenkov, A.P. Rostov, R.Sh. Tsvyk V.E. Zuev Institute of Atmospheric Optics, Siberian Branch, Russian Academy of Sciences, pl. Akad. Zueva 1, 634055 Tomsk, Russia; e-mail: banakh@iao.ru;
V.V. Zhmilevskii, A.B. Ignatiev, V.V. Morozov JSC Almaz-Antey, Leningradskii prosp. 80, korp. 16, 125190 Moscow, Russia

Received 8 July 2014; revision received 30 September 2014
Kvantovaya Elektronika **45** (2) 153–160 (2015)
Translated by Yu.P. Sin'kov

probe laser beams are focused at some distance in atmosphere, while the backscattered probe-beam radiation is recorded in the sharp-image plane tuned to the focal plane. The mean power of the detected probe-beam backscatter signal is used to control the initial wavefronts of the probe and main beams using a deformable (flexible) mirror. The field of view of the detector was taken sufficiently small to provide the desired detector sensitivity to changes in the mean received backscatter power caused by probe beam defocusing due to initial wavefront aberrations [1–4].

A schematic diagram of the experimental setup is shown in Fig. 1. An ideal configuration is depicted, in which the sharp image plane in the receiving telescope is tuned exactly to the beam focal plane, and the transmitter and detector axes are aligned. The probe and main beams are extracted to atmosphere through a round aperture, and detection is performed through a large annular aperture. When compensating for wavefront aberrations using a flexible mirror (FM), the probe-beam transverse sizes in the focal plane change. The beam cross section in the waist is shown as a circle in Fig. 1. The gray circle inside is the area falling in the detector field of view. The beam waist can be located either closer or farther than the focal plane (the distance to which determines the position of the sharp image plane of the detecting system); it can also be displaced from the detector optical axis. An important condition for obtaining a control backscatter signal is as follows: at least a part of the beam cross section in the focal plane must fall in the detector field of view.

Figure 2 shows an optical scheme of the system composed of three main parts: transmitting, detecting and controlling channels. The transmitter includes a pulsed probe laser; a cw laser, forming the main beam; a lens beam expander (collimator); an adaptive mirror; optics for controlling the main-beam wavefront; and a guidance system. The latter is used to align the transmitter and detector optical axes and extract laser beams to atmosphere.

The probe radiation source is a fibre pulsed laser with a wavelength $\lambda = 1.067$ μm (laser 1), and the main beam source is a cw garnet laser with $\lambda = 0.532$ μm (laser 2). Both laser beams are converged using a dichroic plate (DP) beam splitter.

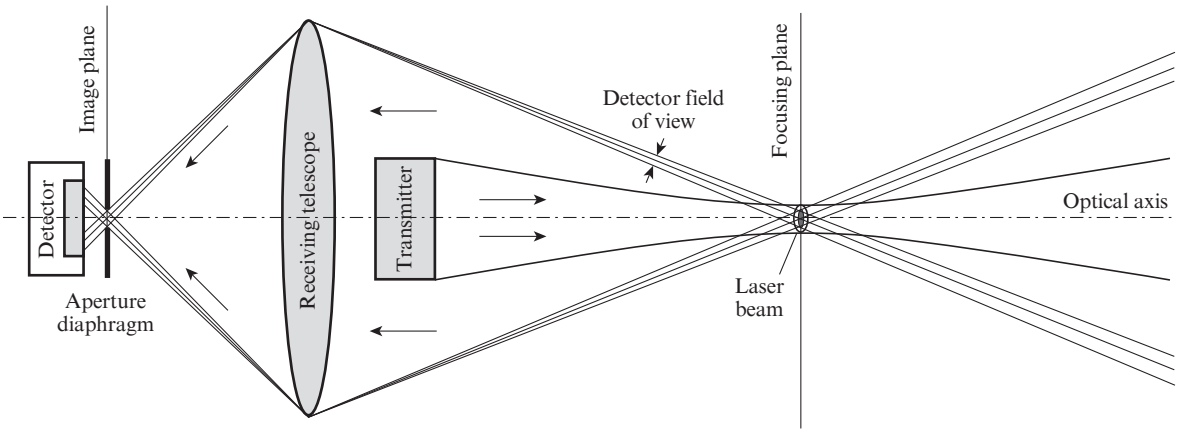

Figure 1. Principle of operation of aperture sounding system.

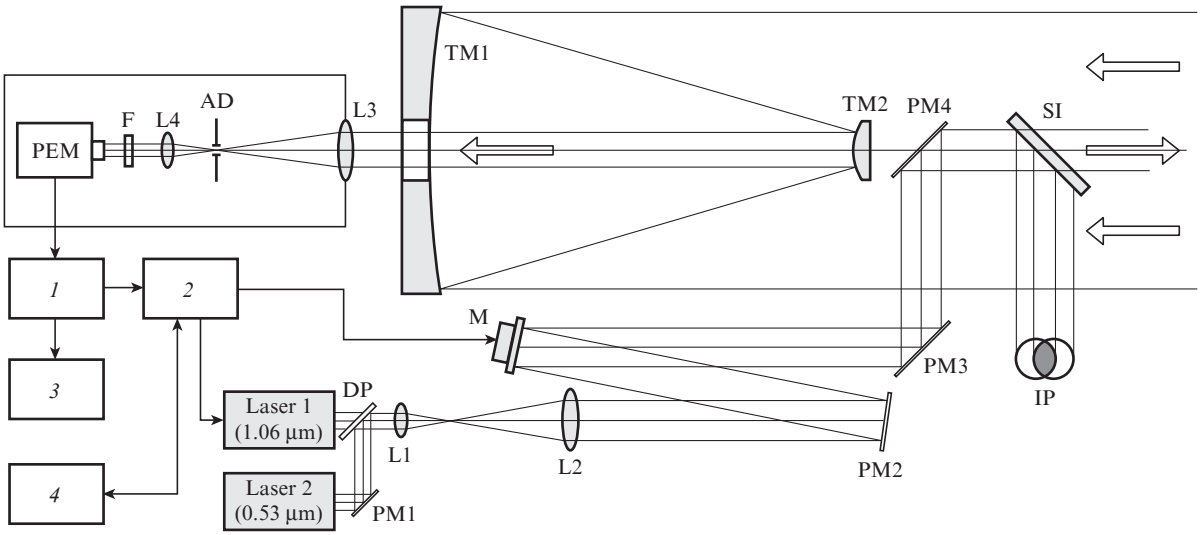

Figure 2. Optical scheme and basic units of the system:
(FM) flexible mirror; (L1–L4) lenses (L1 and L2 form a collimator); (PM1–PM4) plane mirrors; (DP) dichroic plate; (TM1, TM2) main and secondary mirrors of receiving afocal Mersenne telescope; (SI) shearing interferometer; (IP) interference pattern formed by the beam of laser 2; (AD) aperture diaphragm; (IF) interference light filter; (*1*) amplifier; (*2*) controller; (*3*) oscilloscope; (*4*) computer.

Plane mirrors PM1--PM4 can be rotated to locate compactly optical elements on the optical bench and perform necessary alignments. Collinear laser beams are directed to a six-fold lens collimator (composed of lenses L1 and L2) expanding the beams.

After the collimator the beams arrive at an adaptive flexible mirror FM. The collimator, plane mirror PM2 and adaptive mirror FM are arranged so as to make the angle of incidence of the beams arriving at the adaptive mirror maximally close to normal and thus increase the efficiency of compensating for wavefront distortions by the mirror. Mirrors PM3 and PM4 form a periscope, which guides the beams on the axis of the receiving telescope and directs them to atmosphere.

A shearing interferometer SI is installed behind the periscope. It is a 20-mm-thick glass plate with flat faces, converging in the horizontal direction at an angle of 10″. The interferometer forms an interference pattern IP (a set of alternating dark and bright fringes) on the screen. The fringe width is determined by the convergence angle of plate faces, and the inclination angle of the fringes depends on the beam wavefront curvature. A change in the beam focal length in atmosphere leads to a change in the fringe inclination angle in the interference pattern. In the case of a collimated beam with a flat wavefront, the fringes should be oriented along the beam axis.

When the beam wavefront has aberrations, the fringes in the interference pattern are distorted. The degree of pattern distortion depends directly on the degree of the wavefront distortion. Ideally, the work of the adaptive system should result in flat parallel fringes of identical width in the interference pattern.

The receiving system contains a telescope, a former of the detector field of view, a filter of daylight background and a photodetector. The light scattered in atmosphere arrives at the receiving afocal $10^{\times}$ Mersenne telescope 40 cm in diameter, formed by two parabolic mirrors: TM1 and TM2. This telescope is a mirror collimator tuned to a certain distance. A collimated beam 40 mm in diameter, emerging from the telescope, is directed to the receiving box. A former of the detector field of view is located after the telescope; it consists of a focusing lens L3 with a focal length 28 cm, an aperture diaphragm AD 150 μm in diameter, and a collimating lens L4. With allowance for the telescope magnification ($10^{\times}$), the full field-of-view angle is 54 μrad.

Calculations based on the optical design programme Zemax showed that the receiving part of the system provides diffraction quality. At the same time, the transmitting optics, due to intrinsic aberrations, increases the beam divergence beam by 20 μrad. The angular diffraction divergence of a beam with diameter $d = 56$ mm at wavelength $\lambda = 1.06$ μm is about $2.44\lambda/d = 47$ μrad. Thus, the appropriate choice of the detector field-of-view angle in the adaptive system (54 μrad) makes it possible to reduce the angular divergence of the probe beam almost to the diffraction limit.

An interference filter IF and a photoelectron multiplier PEM are installed behind lens L4.

When atmosphere is clean and echo signals are weak, the PEM operates in the photon-counting mode; single-electron electric pulses from the PEM arrive at the amplifier (*1*). At large values of the backscatter coefficient (under conditions of dense atmospheric haze or snowfall), the occurrence rate of single-electron pulses increases, as well as their amplitude, as a result of which the PEM operates in the current detection mode.

A PEM signal arrives at an amplifier and then at a computer-aided controller (*2*) of the adaptive mirror and at the oscilloscope (*3*). The controller supplies a sync pulse to the unit control of the probe laser (is omitted in the figure) and control voltages to adaptive mirror elements; it performs also integration of each echo-signal over distance and summation of echo-signals. Computer *4* is used to drive the controller and oscilloscope; set parameters of SPGD [6, 7], implemented in the controller; carry out initiate adaptation; and graphically visualise it.

Below we present the main parameters of the experimental setup for controlling the initial beam wavefront based on atmospheric backscatter.

Probe radiation transmitter

Mean power/W	50
Wavelength/μm	1.067
Pulse repetition rate/kHz	50
Pulse energy/mJ	1
Pulse duration/ns	200
Beam diameter/mm	56
Beam divergence/μrad	.67

Adaptive mirror

Mirror type	bimorph
Mirror diameter/mm	56
Number of electrodes	57
Voltage range/V	0–600
Shift amplitude/μm	45
Operating frequency/kHz	< 1
Number of channels	32

Controller

Control algorithm	SPGD
Control frequency/Hz	1–500
Signal accumulation time/ms	1.28

Detector

Afocal telescope diameter/cm	40
Effective focal length/mm	2800
Field of view/μrad	54
Detector	PEM
Detector quantum efficiency (%)	2

3. Measurement results

Experiments were performed with main and probe beams focused at a distance of 300 m. The measurement path passed above a rough wooded-urban terrain at heights from 12–15 m in the beginning of the path and up to 50–100 m at a distance of 300 m. The probe pulse energy was 1 mJ; correspondingly, the atmospheric echo-signal was rather weak. Estimations performed for the above parameters showed that, as a result of molecular scattering in surface atmosphere, the number of detected photons per pulse at a distance of 300 m does not exceed 10–15. In this case, we assumed that the loss on each optical surface is 4%, if the optics is not bloomed at $\lambda = 1.06$ μm.

In surface atmosphere, the aerosol backscatter coefficient in the near-IR wavelength range exceeds the molecular backscatter coefficient by approximately an order of magnitude. Due to this, the number of recorded photons per pulse

increases to about 100–150. The detected photon statistics is described by a Poisson distribution, for which the relative signal detection error is equal to the inverse square root of the number of detected photons; hence, for 110–170 photons, detected in total due to molecular and aerosol scattering, the error is about 8%–10% for a single pulse. Since such a large error is intolerable, we averaged echo signals from single pulses to increase the control signal stability.

Figure 3 shows oscillograms of echo signals (detected under haze conditions) from a single pulse and as a result of averaging over $N = 64$ and 1000 laser pulses. The controller integrated the echo-signal at the focusing distance for 1 μs; therefore, the longitudinal size of the scattering volume was 150 m. The first peak is due to spurious scattering from optical and mechanical elements of the measurement setup. It has the same shape as the laser pulse. The second peak is the useful signal from the region located at the focusing distance (300 m). The signal in the oscillogram for $N = 1$ strongly fluctuates; one can see single-electron pulses. Averaging over $N = 64$ yields an acceptable quality of detected signal. In this case, the signal accumulation time is 1.28 ms, and the frequency of the beam wavefront adaptive control using an FM with an operating frequency of 1 kHz can be as high as 780 Hz.

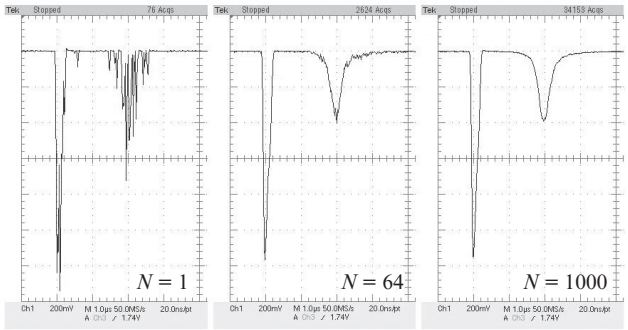

Figure 3. Oscillogram of probe-beam echo signal for a single pulse and for averaging over the number of pulses $N = 64$ and 1000.

Under clean-atmosphere conditions, when the aerosol scattering coefficient is small, the echo signal is weak. Under daylight conditions, the detector signal contains a constant daylight background. Since these factors reduce the signal-to-noise ratio, one must accumulate echo signals and subtract the background after the accumulation. Echo signals obtained without averaging ($N = 1$) and with averaging ($N = 64$ and 1000) are presented in Fig. 4a. At $N = 1$, the signal can hardly be distinguished because of the daylight background. One observes only an irregular set of single-electron pulses with different amplitudes, or continuous bunches of pulses formed at the instants when the PEM current mode is implemented. This noisy signal is absolutely inappropriate for adaptive mirror control; hence, one must perform averaging over some number N of detected echo signals. The choice of N is not unambiguous. Large N values yield high averaging quality but reduce the adaptive-mirror control rate. At small N, the control is impossible because of signal fluctuations.

Averaging over 64 and 1000 echo signals makes it possible to distinguish a signal from the region at the probe-beam focusing distance (300 m) in the oscillograms (Fig. 4a), to which the sharp-image plane of the receiving telescope is tuned. The oscillograms always contain a short spurious pulse

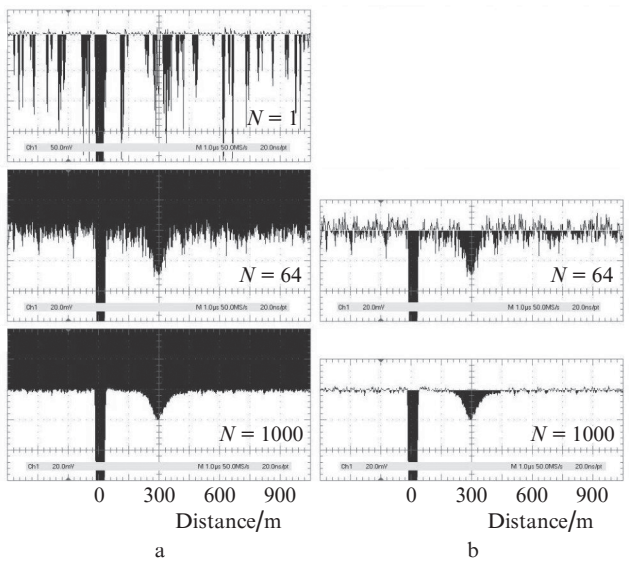

Figure 4. Echo signals obtained in clean atmosphere at different averagings ($N = 1$, 64, and 1000): (a) initial and (b) correlated (with daylight background removed) signals. The measurements were performed on February 28, 2014.

at zero distance. It can be seen that the daylight background forms a pedestal, against which the echo signal is selected. This pedestal is removed by simple subtraction of the corresponding constant from the initial signal. The background level can be determined from a signal received from a large distance, where the useful echo signal is absent.

Figure 5 shows images (made by a Sony video camera) of an IR laser beam ($\lambda = 1.067$ μm) in atmosphere, focused at distances of 200, 300 and 400 m, with the adaptive-mirror control switched off. A beam with the switched-on control is shown in Fig. 5d. The receiving optics for tuned to 300 m in this case; therefore, the system refocused the beam to specifically this distance. Visually, the beam quality increased in comparison with initial, because wavefront distortions, caused

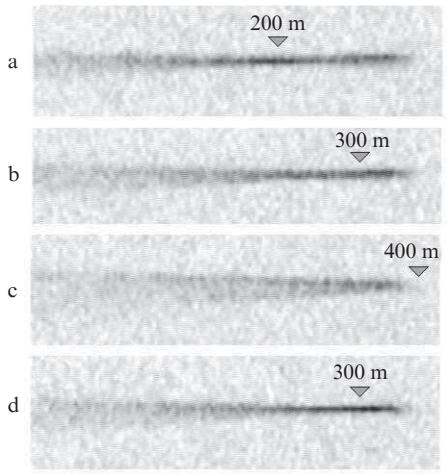

Figure 5. Photographs of the IR laser beam, focused at distances of (a) 200, (b) 300 and (c) 400 m in weakly turbid atmosphere. With the switched-on control (d), the beam converges at the telescope focal distance (300 m).

by transmitting-optics aberrations, were removed during adaptation.

The adaptive mirror was controlled using a specially designed processor: optimisation controller (*2*) in Fig. 2, which implements SPGD. An example of controlling the beam wavefront using this processor is illustrated by Fig. 6, which shows the interface of the program visualising the SPGD operation. Here, and in the similar figures below, the echo-signal amplitude (which increases while wavefront aberrations are compensated for) is plotted along the ordinate axis and the iteration number is plotted along the abscissa axis. A scale division on the abscissa axis corresponds to 1 s. It can be seen that the signal reaches the maximum value for 2 s. The mirror control frequency in the experiment was 250 Hz; thus, it was necessary to perform about 500 algorithm iterations to reach the maximum.

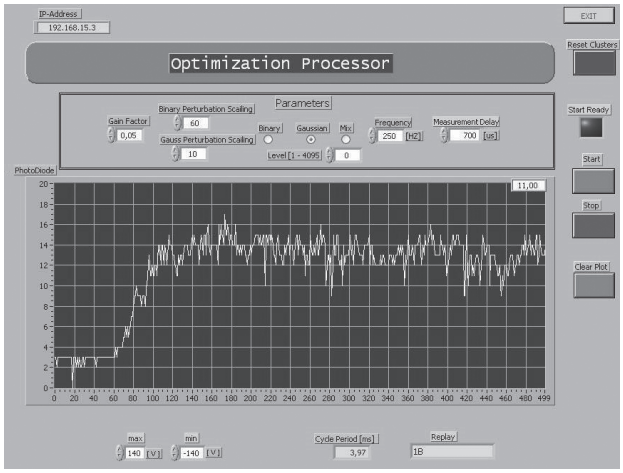

Figure 6. Interface of the program used by the controller to visualise the adaptive mirror control.

The data in Fig. 7 demonstrate the stability of operation of the system for the adaptive contour control. A realisation in which control was absent for the first 5 s and then switched on is shown in Fig. 7a. The signal increased by a factor of 4 for 2 s and remained at this level for a long time. Figure 7b presents a realisation in which voltages on all electrodes were

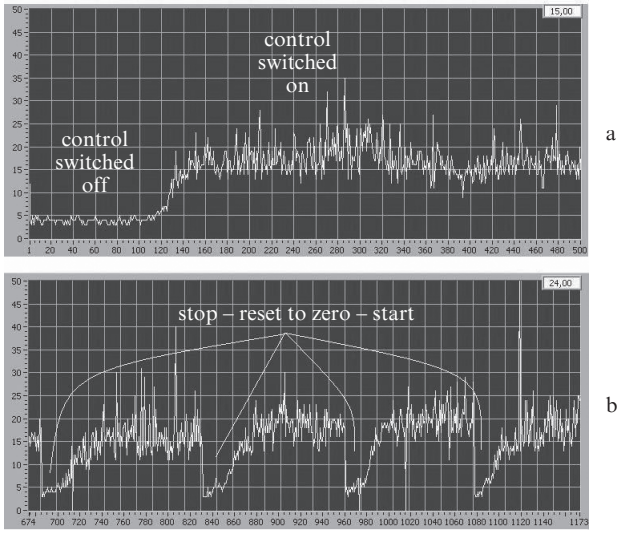

Figure 7. Realisations of FM control signal under clean atmosphere conditions. Data on February 14, 2014.

forcedly nullified (with FM control switched on) approximately each 10 s. This voltage nullification led to misphasing of adaptive-mirror elements, thus inducing artificial distortions of the beam wavefront. Each time the system returned the signal to the previous level, demonstrating stable optimisation controller work.

The changes in the backscatter signal due to backscatter coefficient fluctuations and optical turbulence are shown in Fig. 8, which presents a sequence of echo signals. Echo-signal fluctuations may affect the wavefront control. When backscatter-signal fluctuations caused by atmospheric factors become comparable with random changes in the control-signal amplitude, generated in correspondence with SPGD, the beam wavefront quality cannot be improved any more. This realisation of control signal is illustrated by Fig. 9, which shows also echo-signal profiles and interference patterns of the main beam in the beginning and in the end of realisation. First the control was switched off (during up to 5×10^3 steps), then switched on (after which the signal immediately increased), and finally switched off again (in the middle of realisation). On average, the signal increased by a factor of about 3.5.

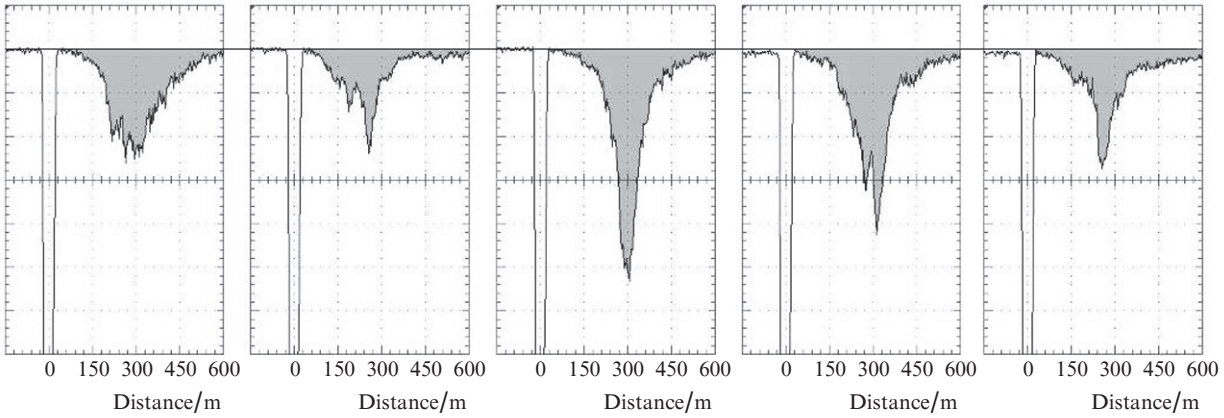

Figure 8. Oscillograms of echo signals detected under conditions of dense atmospheric haze; vertical and horizontal scales are 50 mV div^{-1} and 1 μs div^{-1} (150 m div^{-1}), respectively (data on February 18, 2014).

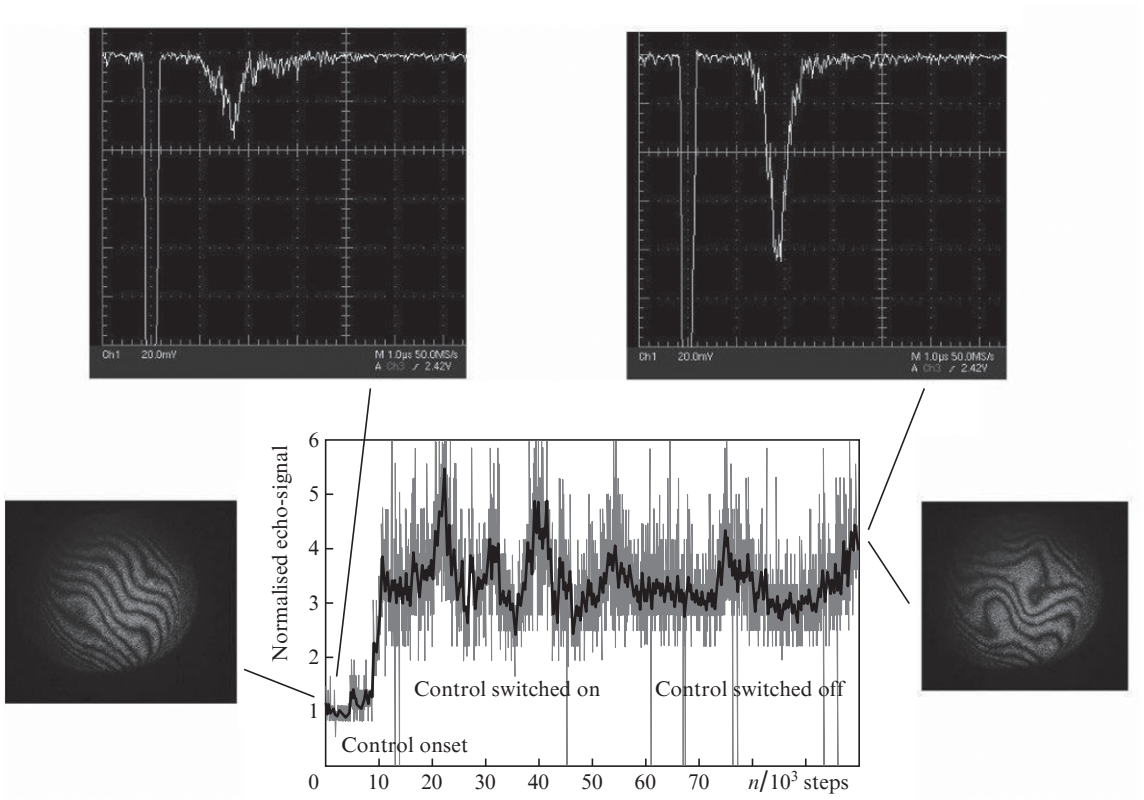

Figure 9. Work of adaptive system under conditions of strong echo-signal fluctuations (data on February 25, 2014); the bold line shows the averaged signal.

During the mirror control the signal strongly fluctuated. After switching off the control, the signal fluctuations decreased but remained rather large. With the control switched on and off, the signal standard deviation was 24 and 21%, respectively. On the assumption of stable atmosphere, the control-induced signal standard deviation was smaller than the standard deviation due to fluctuations of backscatter coefficient and refractive index (21%); it amounted to about 12%. Therefore, the signal stopped increasing.

Typical data of five realisations of control signal measurements; photographs of coaxially propagating probe (laser 1, $\lambda = 1.067$ μm) and main (laser 2, $\lambda = 0.532$ μm) beams in atmosphere under weak snowfall conditions; and interference patterns, visualising the main-beam wavefront, are presented in Fig. 10. Before each realisation, the voltages on FM electrodes were nullified. Each of panels a–e in Fig. 10 presents (from left to right) realisations (30 s long) normalised to the initial value of the control signal; photographs of the beams, focused at a distance of 300 m [equal to the focal length of telescope (1)] and to a distance exceeding the telescope focal length, with FM control switched off (2) and switched on (3); and main-beam interference patterns for the same conditions.

The data in Fig. 10 indicate that laser beams, being initially defocused with the aid of collimator and due to the wavefront aberrations arising at zero voltages on the FM elements, are focused at a specified distance during adaptation. The inclination angle of fringes in the interference pattern visualising the main-beam wavefront first increases with a displacement of the beam focus at distances exceeding 300 m (2); however, then, during FM-aided compensation of aberrations, the inclination of fringes (3) becomes close to initial (1), which is indicative of better beam convergence. The fringes in the interference pattern remain distorted, because the angular resolution of the receiving system (54 μrad) was insufficient to provide detector sensitivity to small-scale aberrations. The application of adaptive system under atmospheric conditions on a surface path led to an increase in the backscatter signal of probe radiation by a factor of more than 4. The backscatter-signal power reaches a maximum value for 3.4 s on average.

4. Conclusions

We experimentally studied the feasibility of adaptive control of the initial wavefront of a laser beam using atmospheric backscatter signal. A laboratory breadboard of the adaptive system was developed, which makes it possible to compensate for aberrations of the initial wavefront of an optical (main) beam by aperture sounding using an atmospheric backscatter signal of an additional probe laser source operating at a different wavelength. The inclination of fringes in the interference pattern visualising the main-beam wavefront changes during the adaptive wavefront control. Introduction of artificial aberrations leads to an increase in the inclination angle; however, during compensation of aberrations using an FM controlled by backscatter signal, the inclination becomes close to initial. The probe backscatter signal may increase by a factor of more than 4 during the FM adaptive control. The breadboard provides the wavefront control under conditions of clean atmosphere, haze and weak or moderate snowfall.

The minimum time for which the control signal reaches a maximum (the time after which maximally possible compensation for wavefront distortions in the main beam is implemented) is 2 s for an FM with a working rate of 1 kHz. On average, the time for which the control signal reaches a maxi-

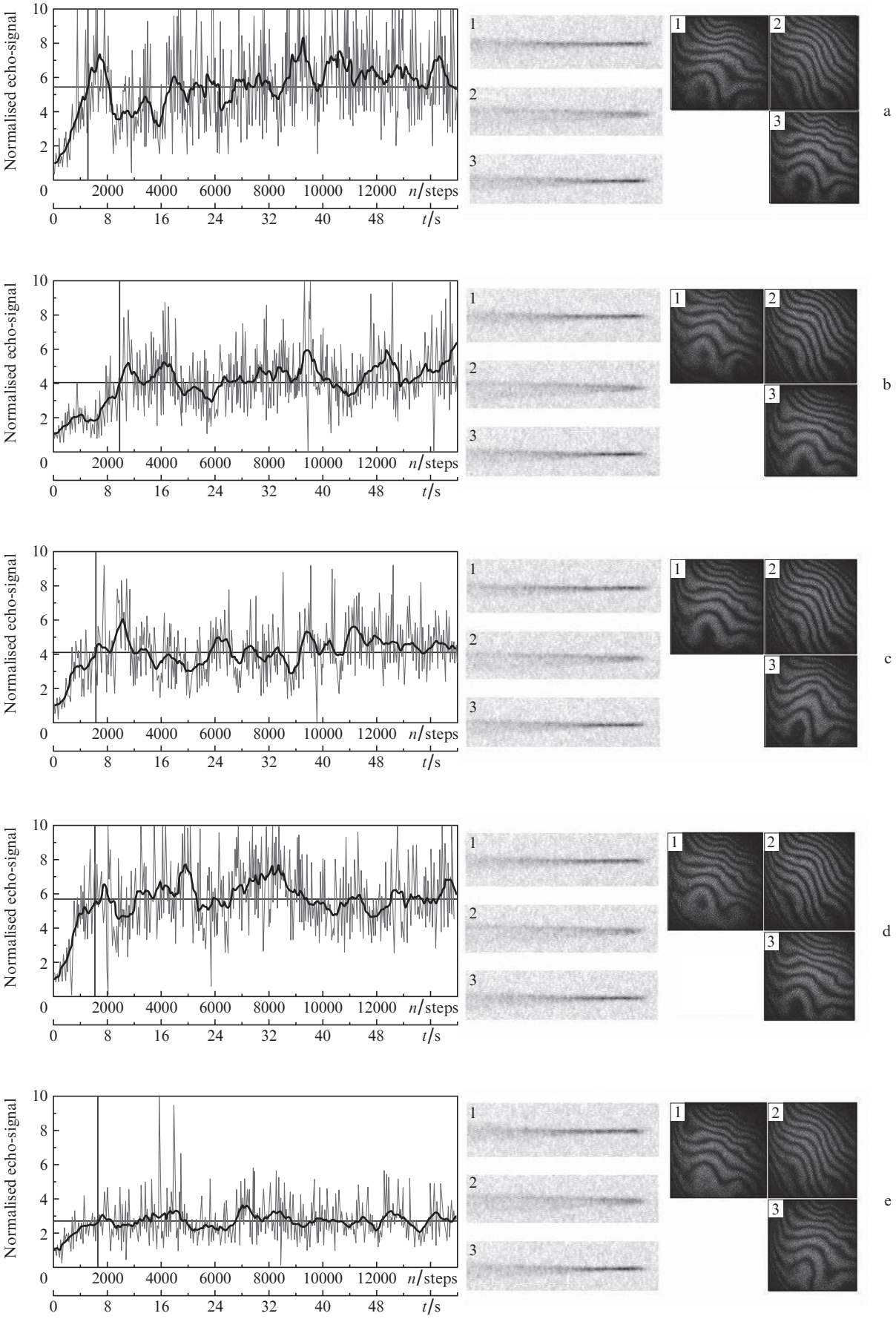

Figure 10. Work of adaptive system; the bold lines show averaged signals.

mum with the aid of this mirror lies within 3–3.5 s. The operational speed of the adaptive contour can be increased by fitting the optimal parameters of the SPGD for the FM control, implemented in the optimisation controller.

Acknowledgements. This work was supported by the Russian Foundation for Basic Research (Grant No. 13-02-98016-r_sibir').

References

1. Zhmilevskii V.V., Ignatiev A.B., Konyaev Yu.A., Morozov V.V. *Abstr. XI Joint Int. Symp. 'Atmospheric and Ocean Optics. Atmospheric Physics'* (Tomsk, 2004) p. 92.
2. Banakh V.A., Zhmilevskii V.V., Ignatiev A.B., Morozov V.V., Rychkov D.S. *Kvantovaya Elektron*., **38**, 764 (2008) [*Quantum Electron*., **38**, 764 (2008)].
3. Banakh V.A., Zhmilevskii V.V., Ignatiev A.B., Morozov V.V., Smalikho I.N. *Opt. Spektrosk*., **108**, 113 (2010).
4. Banakh V.A., Zhmilevskii V.V., Ignatiev A.B., Morozov V.V., Smalikho I.N. *Opt. Spektrosk*., **111**, 488 (2011).
5. Banakh V.A., Zhmilevskii V.V., Ignatiev A.B., Morozov V.V., Tsvyk R.Sh., Shesternin A.N. *Opt. Atmos. Okeana*, **26**, 1023 (2013).
6. Vorontsov M.A., Sivokon V.P. *J. Opt. Soc. Am.*, **15**, 2745 (1998).
7. Banakh V.A., Larichev A.V., Razenkov I.A., Shesternin A.N. *Opt. Atmos. Okeana*, **25**, 1099 (2012).
8. Vorontsov M.A., Shmal'gauzen V.I. *Printsipy adaptivnoi optiki* (Principles of Adaptive Optics) (Moscow: Nauka, 1985).
9. Tyson R.K. *Principles of Adaptive Optics* (Boston, MA: Academic Press, 1998).